Continuous Monitoring of a Path-Constrained Moving Target by Multiple UAVs

Camilla Tabasso *, Calvin‘ Kielas-Jensen † and Venanzio Cichella ‡
University of Iowa, Iowa City, IA, 52242

Satyanarayana Manyam§
Infoscitex corp., a DCS company, Dayton, OH, 45431

David W. Casbeer¶, and Isaac Weintraub‖
Air Force Research Laboratory, Wright-Patterson AFB, OH, 45433

In this work, a continuous monitoring scenario where multiple UAVs are tasked to monitor a dynamic target moving along a path with unknown speed profile is addressed. Optimal trajectories based on the nominal trajectory of the target are generated offline. If changes in the speed profile of the target are detected, the agents' trajectories can be modified online to ensure that the monitoring requirements are met, while still maintaining inter-vehicle safety guarantees. The time-coordination algorithm proposed as a solution to this problem is based on a leader-follower structure. The UAVs are assumed to exchange information over a communication network where limited quality of service, switching topologies and data package dropouts are considered. Finally, performance bounds and simulation results to prove the efficacy of our method are provided.

I. Introduction

Multi-vehicle missions have increasingly gained popularity in the last few decades for both civil and military applications because of their many advantages. The deployment of multiple agents can be particularly useful in applications that require the coverage of large areas such as in surveillance missions [1–3]; environmental monitoring [4–6]; and sweeping tasks [7]. Often, such tasks cannot be performed by stationary agents given the changing nature of the environment. Instead, it is preferred to deploy teams of unmanned vehicles that work cooperatively to monitor the desired target or area. In the literature, this cooperative approach is often referred to as monitoring [8, 9].

In this work, we address a continuous monitoring scenario where multiple Unmanned Aerial Vehicles (UAVs) are tasked to monitor a target travelling with an unknown speed along a known predefined path. Specifically, the agents are

*Graduate student, Department of Mechanical Engineering, camilla-tabasso@uiowa.edu.
†Graduate student, Department of Mechanical Engineering, calvin-kielas-jensen@uiowa.edu.
‡Assistant Professor, Department of Mechanical Engineering, venanzio-cichella@uiowa.edu, AIAA Member.
§Research Scientist, msngupta@gmail.com, AIAA member.
¶Research Engineer, Control Science Center of Excellence, david.casbeer@us.af.mil, AIAA Associate Fellow.
‖Research Engineer, Aerospace Systems Directorate, isaac.weintraub.1@us.af.mil, AIAA Member.

equipped with sensors fixed to their body and the mission requires the target to be within the sensing footprint of at least one UAV at all times. Due to limitations on the range of the sensors, this is satisfied by requiring the agents to fly over the target at specific times. Furthermore, the agents are required to coordinate in order to guarantee inter-vehicle safety and successful completion of the monitoring mission while adhering to feasibility constraints such as minimum and maximum speed and angular rates.

In terms of previous work, many approaches to monitoring and surveillance-like missions can be found in the literature. In [10], a scenario where multiple vehicles are required to visit a set of discrete locations is considered. The authors formulate their solution as a vehicle routing problem with time windows. In [11], the authors propose a solution to a similar problem by implementing a routing algorithm for persistent monitoring of targets with weighted revisit priorities. In [12, 13], the authors formulate an optimal control problem to minimize the cumulative uncertainty of the sensing points. In [12], the persistent monitoring problem is addressed for a one-dimensional space, whereas in [13], the same approach is extended to a two-dimensional space. In [14], the authors propose a method to patrol an area with the presence of static targets while driving the uncertainty of the targets to zero.

The presence of dynamic targets poses an extra challenge, because it is necessary to detect if the target is deviating from its nominal trajectory and adjust the agents' trajectories accordingly. Existing solutions to this problem are based on closed-loop controllers and allow the agent to react in real time to stochastic behaviour of the target [15, 16]. In [15, 16], for example, the authors propose an optimal feedback controller to track a Brownian target where the agent is modeled as Dubins vehicle. These closed-loop approaches have several advantages, including obstacle avoidance and computational efficiency. Nevertheless, they can be too conservative when dealing with complex mission scenarios, such as nonconvex problems, multi-agent missions where inter-vehicle safety measures need to be guaranteed, or in the presence of nonlinear vehicle dynamics. To address these issues, the monitoring problem can be formulated as a constrained nonlinear optimal control, that can be solved in an open-loop fashion using numerical methods [17–19]. The main advantages include: (*i*) complex constraints such as inter-vehicle safety, feasibility and flyability of the trajectory, and nonlinear vehicle dynamics can be taken into account; (*ii*) the open-loop approach enhances human operator trust through transparent and predictable operations, since the solution is generated in one shot for a long temporal window. The main drawback to the sole use of open-loop numerical techniques for the solution of optimal control problems lies in the fact that replanning trajectories is computationally expensive and may require a substantial amount of time. For monitoring applications, this can be undesirable because the target may frequently change its speed as a defense technique and, therefore, it may result in loss of performance.

To address the limitations mentioned above, we introduce a hybrid solution. We decouple the continuous monitoring problem into an offline optimal trajectory generation and a time-coordination algorithm for online trajectory adjustment. Our approach departs from previous methods in the sense that an optimal motion planner is exclusively utilized before the beginning of the mission to generate trajectories based on the nominal knowledge of the trajectory of the target.

During the mission, the UAVs can cooperatively adjust their trajectory online to take into account bounded variations in the speed profile of the target. In doing so, they can avoid replanning their trajectories while still being able to track their target.

Building up from previous work [20–23], we focus on the time-coordination algorithm for online trajectories adjustment. In [20], the authors propose an algorithm that requires the vehicles to coordinate according to a common temporal objective established at the beginning of the mission, whereas in [21, 22] the temporal objective can be modified during the mission to satisfy mission requirements, e.g., collision avoidance. These algorithms are based on mild assumptions on the communication network and take into account communication dropouts and switching topologies. Extending the work presented in [23], we propose a time-coordination algorithm based on a leader-follower structure. This choice was motivated by the fact that, conversely to the methods mentioned above, our approach requires only a subset of vehicles, the mission leaders (or virtual leaders), to have the necessary equipment to detect the position of the target along a path. Then, persistent monitoring by the fleet is enabled by means of communication of limited information among the vehicles. This assumption allows more flexibility in terms of hardware and sensors needed on-board the followers, which is more realistic, and it allows a decrease in the overall costs of the mission. For example, this method can be useful in scenarios where one leader can detect the position of the target using radar's measurements, while the followers are equipped with only a camera for monitoring the target.

This paper is organized as follows: the cooperative framework that motivates the continuous monitoring problem of this paper is discussed in Section II. The mathematical formulation of the problem itself is provided in Section III. Section IV presents the main result and the continuous monitoring algorithm is presented in Section V. Finally, a demonstration of the efficacy of the algorithm is provided in Section VI. Conclusions are included in Section VII.

II. Cooperative Control Framework

The cooperative control framework this work is based on includes (*i*) a trajectory generation algorithm for the offline planning of optimal trajectories [24–26]; (*ii*) a virtual target tracking algorithm that ensures the vehicles are able to follow their desired trajectories [27, 28]; and (*iii*) a time-coordination algorithm that indirectly adjusts the speed of the vehicles online to guarantee coordination and satisfaction of the mission requirements. The cooperative control framework is shown is Figure 1. In this work, the focus is on time-coordination, but for the sake of completeness, we briefly introduce the trajectory generation and virtual target tracking algorithms.

Note that for the rest of this paper, we denote vectors with bold letters (e.g., $\mathbf{x} = [x_1, x_2, \ldots, x_n] \in \mathbb{R}^n$), matrices with uppercase letters (e.g., A) and $||\cdot||$ denotes the Euclidean two-norm or magnitude (e.g. $\|\mathbf{x}\| = \sqrt{x_1^2 + x_2^2 + \ldots + x_n^2}$) . Furthermore, $\mathbf{p}_i(t)$ indicates the nominal trajectory of the ith vehicle, whereas $\hat{\mathbf{p}}_i(t)$ refers to the actual trajectory of the ith vehicle.

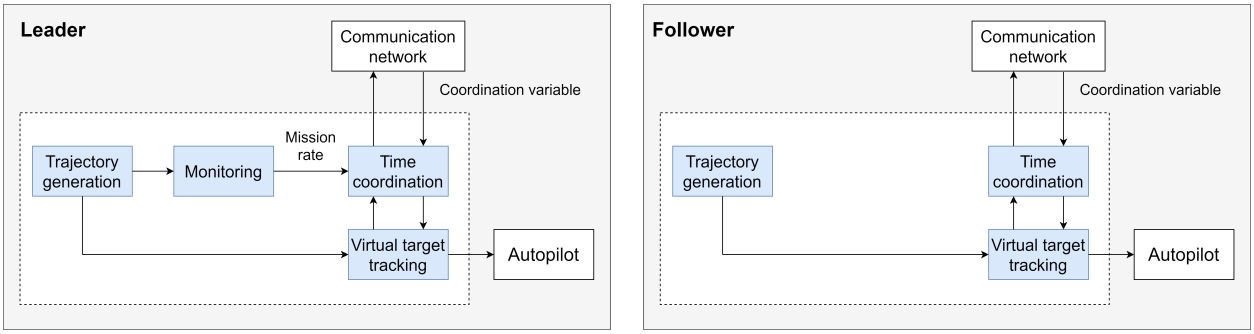

Fig. 1 Cooperative Control Framework.

A. Trajectory Generation

At the motion planning level, trajectory generation is formulated as an optimal control problem. The objective is to generate trajectories for the vehicles that satisfy safety constraints, boundary conditions, feasible constraints and mission specific constraints.

For safety constraints, minimum temporal separation requirements are enforced to generate collision-free trajectories. Specifically, the trajectories are generated such that the following holds:

$$||\mathbf{p}_i(t) - \mathbf{p}_j(t)|| \geq d_{\text{safe}}, \quad \forall \quad t \in \mathbb{R}, i, j \in \{1, .., n\}, i \neq j. \tag{1}$$

Boundary conditions include the initial and final position and initial and final heading angle. The feasible constraints concern minimum and maximum velocity and angular rate saturation limits. Finally, the mission specific constraints depend on the mission under consideration, namely continuous monitoring. To accomplish the mission, the vehicles are required to sequentially intercept the target at constant time samples Δ, i.e.

$$||\mathbf{p}_i(i\Delta) - \mathbf{p}_t(i\Delta)|| \leq \epsilon, \quad i \in \{1, .., n\}, \tag{2}$$

where $\mathbf{p}_i(i\Delta)$ and $\mathbf{p}_t(i\Delta)$ are the positions of the ith vehicle and target, respectively, at $t = i\Delta$, and ϵ is a relaxation bound. We note that *intercepting* means that the ith vehicle is flying over the target. Furthermore, with this formulation each vehicle intercepts the target once at its corresponding time sample. For missions with long time horizons or extending over large areas, the vehicles may be required to intercept the target multiple times to ensure that it is still within their sensor footprint. For these cases, a trajectory replan can be triggered to extend the original trajectories.

The optimal trajectories are generated in 2 dimensions; the altitude of the vehicles is controlled separately. Furthermore, to avoid detection or defensive maneuvers, the vehicles are required to approach the target at a random heading angle

$$\psi_i(i\Delta) = \theta_i, \qquad i \in \{1, 2, \ldots, n\},$$

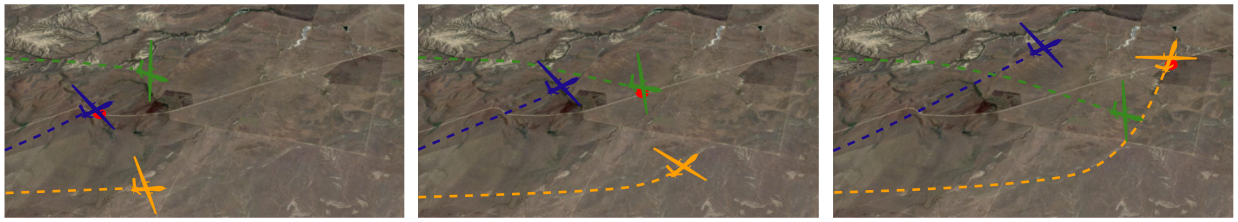

Fig. 2 Persistent monitoring scenario in which target detection is performed by three UAVs.

where $\psi_i(i\Delta)$ is the heading angle of the ith vehicle at $t = i\Delta$, and θ_i is a uniformly randomly generated angle. Figure 2 illustrates the objectives of the continuous monitoring mission. Each of the UAVs, shown in blue, green and yellow, intercept the trajectory of the target, shown in red. Furthermore, the vehicles approach the target at different heading angles.

The trajectory generation problem can be stated as follows:

Problem 1 *Consider a mission involving n vehicles. Compute a set of n feasible trajectories* $\boldsymbol{p}_i(t) : [0, t_f] \rightarrow \mathbb{R}^2$, $i = 1, 2, \ldots, n$, *that minimize a given cost function J and satisfy the vehicles' dynamic constraints, safety constraints, boundary conditions, feasible constraints, and mission specific constraints, i.e,*

$$\min_{\substack{\boldsymbol{x}(t)=[x_1(t),\cdots,x_n(t)]^T \\ \boldsymbol{u}(t)=[u_1(t),\cdots,u_n(t)]^T}} \quad J(\boldsymbol{x(t)}, \boldsymbol{u(t)})$$

subject to

$$\begin{aligned}
\dot{\boldsymbol{x}}_i(t) &= \boldsymbol{f}(\boldsymbol{x}_i(t), \boldsymbol{u}_i(t)), \\
\boldsymbol{p}_i(t) &= \boldsymbol{g}(\boldsymbol{x}_i(t)), \\
u_{\boldsymbol{min}} \leq ||\boldsymbol{u}_i(t)|| &\leq u_{\boldsymbol{max}}, \\
\boldsymbol{p}_i(0) &= \boldsymbol{p}_{i,0}, \\
\boldsymbol{p}_i(t_f) &= \boldsymbol{p}_{i,t_f}, \\
\psi_i(0) &= \psi_{i,0}, \\
\psi_i(t_f) &= \psi_{i,t_f}, \\
||\boldsymbol{p}_i(t) - \boldsymbol{p}_j(t)|| &\geq d_{\boldsymbol{safe}}, \\
||\boldsymbol{p}_i(i\Delta) - \boldsymbol{p}_t(i\Delta)|| &= \epsilon, \\
\psi_i(i\Delta) &= \theta_i,
\end{aligned}$$

for all $i, j \in \{1, 2, \ldots, n\}$, $i \neq j$.

To solve the above problem, we adopt the approach presented in [29]. We approximate the states of the vehicles and the inputs by Nth order Bernstein polynomials as follows:

$$x_i(t) \approx \sum_{j=0}^{N} \bar{x}_i^{[j]} b_{j,N}(t), \quad u_i(t) \approx \sum_{i=0}^{N} \bar{u}_i^{[j]} b_{j,N}(t),$$

where $\bar{x}_i^{[j]}$ and $\bar{u}_i^{[j]}$, $j \in \{0, \ldots, N\}$, are polynomial coefficients, and $b_{j,N}(t)$ are Bernstein polynomial basis functions. This approximation allows us to rewrite the functionals involved in Problem 1 as a set of algebraic constraints, dependent on the new optimization variables, namely a finite set of polynomial coefficients. Thus, the optimal control problem given above can be reformulated as a finite dimensional optimization problem, which can be solved using off-the-shelf optimization solvers (e.g., Matlab *fmincon*). The output of the algorithm is a set of optimal coefficients $\bar{x}_i^{[0]}, \ldots, \bar{x}_i^{[N]}$, $\bar{u}_i^{[0]}, \ldots, \bar{u}_i^{[N]}$, which give the optimal polynomial trajectory

$$p_i(t) = \sum_{j=0}^{N} g(\bar{x}_i^{[j]}) b_{j,N}(t).$$

Further details on this method can be found at [29].

B. Virtual Target Tracking Algorithm

Let $\mathbf{p}_i(t)$ be the trajectory of the ith vehicle given by the trajectory generation algorithm. Moreover, let the virtual time $\gamma(t)$ be a temporal variable

$$\gamma_i : \mathbb{R}^+ \rightarrow [0, t_f], \quad \forall \quad i = 1, \ldots, n, \quad t \geq 0. \tag{3}$$

Then, let the vehicles' trajectories be reparameterized in terms of the virtual time, i.e., $\mathbf{p}_i(\gamma_i(t))$. For clarity, we refer to $\mathbf{p}_i(\gamma_i(t))$ as the *virtual target* to be tracked by the ith UAV. With this formulation, the virtual time $\gamma_i(t)$ indirectly represents the progression of the ith vehicle along its planned trajectory. Furthermore, its derivative $\dot{\gamma}_i(t)$ indicates the pace of the mission of the ith vehicle.

Conversely to the clock time t, the virtual time is a quantity that can be stretched or compressed. We note that $\dot{\gamma}(t) = 1$ implies that the mission is progressing at the pace that was originally planned at the trajectory generation level, i.e., $\mathbf{p}_i(\gamma_i(t)) = \mathbf{p}_i(t)$; $\dot{\gamma}(t) \geq 1$ ($\dot{\gamma}(t) \leq 1$) implies a faster (slower) execution of the mission. Later it will be shown that $\gamma(t)$ and $\dot{\gamma}(t)$ play a key role in the execution of the mission as they are used by the time-coordination and continuous monitoring algorithms to indirectly adjust the speed of the vehicles. Therefore, the vehicles' trajectories are feasible if

they solve Problem 1 and if the following bounds hold:

$$1 - \dot{\gamma}_{i,\max} \leq \dot{\gamma}_i(t) \leq 1 + \dot{\gamma}_{i,\max}, \tag{4}$$

$$|\ddot{\gamma}_i(t)| \leq \ddot{\gamma}_{i,\max} \tag{5}$$

with $0 < \dot{\gamma}_{i,\max} < 1$ and $\ddot{\gamma}_{i,\max} > 0$.

Finally, the virtual target tracking problem can be stated as follows.

Problem 2 *Consider n trajectories* $\mathbf{p}_1(\gamma_1(t)), \ldots, \mathbf{p}_n(\gamma_n(t))$ *that solve Problem 1 with virtual times* $\gamma_1(t), \ldots, \gamma_n(t)$ *satisfying Equations* (4) *and* (5)*. Let the virtual target tracking error for vehicle i, namely* $\mathbf{x}_{PF,i}(t)$*, be defined as the difference between the desired and actual position of the ith vehicle, i.e.,*

$$\mathbf{x}_{PF,i}(t) = \mathbf{p}_i(\gamma_i(t)) - \hat{\mathbf{p}}_i(t),$$

where $\hat{\mathbf{p}}_i(t)$ *is the actual position of the ith vehicle at time t. Then, design a control law for the vehicle control inputs such that* $\mathbf{x}_{PF,i}(t)$ *converges to a neighborhood of 0.*

We emphasize that safety and feasibility constraints are first imposed at the motion planning level. Then, the bounds in Equations (4) and (5) guarantee that the virtual targets, i.e., $\mathbf{p}_1(\gamma_1(t)), \ldots, \mathbf{p}_n(\gamma_n(t))$, can be tracked by the vehicles using some trajectory tracking or path following algorithm for fixed-wing UAVs. As an example, we refer the reader to [30].

III. Time Coordination Algorithm - Problem Formulation

As mentioned in the previous section, a trajectory generation algorithm is adopted to create feasible paths. Furthermore, a virtual target tracking algorithm is enabled to allow the vehicles to follow their desired trajectories. Finally, the proposed time-coordination algorithm is applied to guarantee coordination and inter-vehicle safety. In this section, we first introduce the necessary variables and then we formally state the time-coordination problem.

Recall that at the motion planning level, trajectories are generated such that temporal separation requirements are met (see Equation (1)). Furthermore, recall that the trajectories are reparameterized in terms of the virtual time $\gamma(t)$, i.e., $\mathbf{p}_i(\gamma_i(t))$. Notice that if $\gamma_i(t) = \gamma_j(t) \quad \forall i, j \in \{1, ..., n\}, i \neq j$, then inter-vehicle safety is guaranteed throughout the mission. In other words, if coordination is achieved, then inter-vehicle safety is ensured. Moreover, to satisfy the requirements given by the monitoring scenario, $\dot{\gamma}_i(t)$ must converge to $\dot{\gamma}_d(t)$, where the latter is the desired pace of the mission required to successfully intercept the target. For our purposes, $\dot{\gamma}_d(t)$ is a coordination parameter that can be

adjusted online to react to bounded variations in the speed profile of the target. As it was mentioned previously, it is more realistic to assume that only a subset of the agents is capable of detecting the position of the target. Therefore $\dot{\gamma}_d(t)$ is computed by the leaders based on the virtual time of the target, $\gamma_t(t)$. The latter can be calculated as

$$\gamma_t(t) = \eta_t(\ell'_t),$$

where ℓ'_t is the normalized curvilinear abscissa of the target at time t and η_t is a strictly increasing function. Then, $\dot{\gamma}_d(t)$ acts as a reference for the followers which, as it will be clear later, ensures that the monitoring objectives are met by all vehicles. For more details on how $\gamma_t(t)$ is calculated, see Section II.B of [28].

Remark 1 *In this work, we assume that the leaders are always able to detect the position of the target and can compute the virtual time of the target in real time.*

Finally, the time-coordination objectives can be stated as follows:

$$\gamma_i(t) = \gamma_j(t), \quad \forall \quad i, j \in \{1, .., n\}, i \neq j, \tag{6}$$

$$\dot{\gamma}_i(t) = \dot{\gamma}_d(t), \quad \forall \quad i \in \{1, .., n\}. \tag{7}$$

We note that because $\dot{\gamma}_d(t)$ is not known by the followers, the objective of the time-coordination algorithm is to ensure that Equations (6) and (7) are satisfied for *all* vehicles.

To achieve the time-coordination objectives, the communication system plays a key role. Using graph theory, we can model the communication network through which the agents can communicate. Specifically, let $L(t) \in \mathbb{R}^{n\times n}$ be the Laplacian matrix for the time-varying communication graph $\Gamma(t)$ [31] and recall that $\Gamma(t)$ is connected if and only if the second smallest eigenvalue, also known as the Fiedler value of $L(t)$, is strictly positive. Moreover, let $Q \in \mathbb{R}^{(n-1)\times n}$ be a matrix that satisfies the following:

$$Q\mathbf{1_n} = \mathbf{0}\,, \quad QQ^\top = I_{n-1}\,, \quad Q^\top Q = I_n - \frac{1}{N}\mathbf{1_n}\mathbf{1_n}^\top, \tag{8}$$

Remark 2 *An iterative procedure to compute the matrix Q is presented in [27].*

Let $\bar{L}(t) = QL(t)Q^\top$. Here $\bar{L}(t)$ is a matrix with the same eigenvalues as the Laplacian matrix, with the exception of the first eigenvalue of $L(t)$, $\lambda_1 = 0$, which is the eigenvalue associated with the eigenvector $\mathbf{1_n}$. In other words, the smallest eigenvalue of $\bar{L}(t)$ is the Fiedler value of $L(t)$, i.e., $\lambda_1(\bar{L}(t)) = \lambda_2(L(t))$. Then, it can be easily seen that the communication graph $\Gamma(t)$ is connected at time t if $\bar{L}(t)$ is positive definite. We note that this formulation highlights

the dependency of the graph's connectivity on the Fiedler value. In contrast, the following is assumed in terms of the communication graph:

1) The ith vehicle can only communicate with neighboring set of vehicles, here referred to as $\mathcal{N}_i(t)$.
2) The communication between the vehicles is bidirectional and with no time delays.
3) The connectivity of the communication graph $\Gamma(t)$ satisfies a persistency of excitation (PE)-like condition [32]:

$$\frac{1}{nT}\int_{t}^{t+T} \bar{L}(\tau)d\tau \geq \mu I_{n-1}, \qquad t \in [0,\infty), \tag{9}$$

with $T > 0$ and $\mu = (0, 1]$.

Notice that $\mu \in (0, 1]$ follows from the fact that $||\bar{L}|| \leq n$. The connectivity assumption presented in Equation (9) requires the graph to be connected in a integral sense and thus it captures communication dropouts and switching topologies.

Finally, the time-coordination objectives presented in Equations (6) and (7) can be recast into the time-coordination error vector as follows:

$$\mathbf{x_{TC}}(t) = \begin{bmatrix} \boldsymbol{\xi}(t) \\ \mathbf{z}(t) \end{bmatrix}, \tag{10}$$

where

$$\boldsymbol{\xi}(t) = Q\boldsymbol{\gamma}(t), \tag{11}$$

$$\mathbf{z}(t) = \dot{\boldsymbol{\gamma}}(t) - \dot{\gamma}_d(t)\mathbf{1_n}, \tag{12}$$

with $\boldsymbol{\gamma}(t) = [\gamma_1(t), \ldots \gamma_n(t)]^\top$, $\dot{\boldsymbol{\gamma}}(t) = [\dot{\gamma}_1(t), \ldots \dot{\gamma}_n(t)]^\top$.

Then, the objective of the time-coordination algorithm is to design control laws for $\ddot{\gamma}_i(t)$ such that the time-coordination error vector converges to a neighborhood of 0, which in turn implies that Equations (6) and (7) are not violated.

Remark 3 *According to the properties of matrix Q,* $\boldsymbol{\xi}(t) = 0$ *implies* $\gamma_i(t) = \gamma_j(t), i \neq j$ *(see Equation* (8)*), while* $z(t) = 0$ *indicates that* $\dot{\gamma}_i(t) = \dot{\gamma}_d(t)$.

Finally, the time-coordination problem for the fleet of vehicles can be stated as follows.

Problem 3 *Consider a cooperative mission where n UAVs are tasked to coordinate along nominal trajectories that satisfy Problem 1, and are equipped with a virtual target tracking algorithm that satisfies Problem 2. Let the vehicles communicate through a network that satisfies the condition in Equation* (9)*, and that the desired pace of the mission* $\dot{\gamma}_d(t)$ *is known to a subset of* $n_l < n$ *vehicles elected as leaders. Then, the objective of the time-coordination algorithm is to design a control law such that the time-coordination error vector converges to 0 (see Remark 3) and such that inequalities* (4) *and* (5) *are not violated.*

IV. Time Coordination - Main Results

To solve Problem 3, let $\ddot{\gamma}_i(t)$ be governed by

$$\begin{aligned}
&\ddot{\gamma}_i(t) = -b\left(\dot{\gamma}_i(t) - \dot{\gamma}_d(t)\right) - a\sum_{j\in\mathcal{N}_i(t)}\left(\gamma_i(t) - \gamma_j(t)\right), \\
&\qquad\qquad \forall i \in \{1,\dots,n_l\}, \\
&\ddot{\gamma}_i(t) = -b\left(\dot{\gamma}_i(t) - \chi_{I,i}(t)\right) - a\sum_{j\in\mathcal{N}_i(t)}\left(\gamma_i(t) - \gamma_j(t)\right), \\
&\dot{\chi}_{I,i}(t) = -k\sum_{j\in\mathcal{N}_i(t)}\left(\gamma_i(t) - \gamma_j(t)\right), \quad \forall i \in \{n_l+1,\dots,n\}, \\
&\gamma_i(0) = 0, \qquad \dot{\gamma}_i(0) = 1, \qquad \chi_{I,i}(0) = 1,
\end{aligned} \tag{13}$$

which can be written in matrix form as

$$\begin{aligned}
&\ddot{\boldsymbol{\gamma}}(t) = -aL\boldsymbol{\gamma}(t) - b\begin{bmatrix} D^\top\dot{\boldsymbol{\gamma}}(t) - \dot{\gamma}_d(t)\mathbf{1}_{\mathbf{n_l}} \\ C^\top\dot{\boldsymbol{\gamma}}(t) - \boldsymbol{\chi_I}(t) \end{bmatrix}, \\
&\dot{\boldsymbol{\chi}}_{\boldsymbol{I}}(t) = -kC^\top L\boldsymbol{\gamma}(t), \\
&\boldsymbol{\gamma}(0) = \mathbf{0_n}, \qquad \dot{\boldsymbol{\gamma}}(0) = \mathbf{1_n}, \qquad \boldsymbol{\chi_I}(0) = \mathbf{1_{n-n_l}},
\end{aligned} \tag{14}$$

where

$$C^\top = \begin{bmatrix} 0 & I_{n-n_l} \end{bmatrix}, \tag{15}$$

$$D^\top = \begin{bmatrix} I_{n_l} & 0 \end{bmatrix}, \tag{16}$$

and a, b and k are positive coordination control gains. $\dot{\gamma}_d(t)$ is a desired mission pace satisfying

$$1 - \dot{\gamma}_{d,\max} \leq \dot{\gamma}_d(t) \leq 1 + \dot{\gamma}_{d,\max}, \tag{17}$$

$$|\ddot{\gamma}_d(t)| \leq \ddot{\gamma}_{d,\max}, \tag{18}$$

for some $\dot{\gamma}_{d,\max} > 0$ and $\ddot{\gamma}_{d,\max} > 0$. The control laws shown in Equation (13) are designed such that $\dot{\gamma}_i(t) - \dot{\gamma}_d(t) \approx 0$ and $\gamma_i(t) - \gamma_j(t) \approx 0$. Then, using the properties of matrix Q, see Equation (8), it can be shown that this implies that the time-coordination error vector also converges to a neighborhood of 0, thus satisfying the time-coordination objectives presented in (6) and (7). Recall that the coordination parameter $\dot{\gamma}_d(t)$ is known only by the leaders. Therefore, the term $\boldsymbol{\chi_I}(t)$ represents the pace of the mission for the followers and it is used to guarantee that the time-coordination objectives are satisfied for all vehicles.

Theorem 1 *Consider a cooperative mission involving n UAVs, where n_l vehicles are elected as leaders and $n - n_l$ are followers. Let the vehicles be equipped with a trajectory generation algorithm that solves Problem 1 and a virtual target tracking algorithm that solves Problem 2. Assume that the vehicles are able to communicate through a network satisfying Equation* (9)*, and that $\dot{\gamma}_d(t)$ is known by the leaders only. Finally, let $\ddot{\gamma}_i(t)$ be governed by the control law presented in* (14)*, and the time-coordination error vector $\mathbf{x_{TC}}(t)$ at time $t = 0$, and the dynamic limits of the desired mission pace satisfy*

$$\dot{\gamma}_{d,\max} < \dot{\gamma}_{i,\max}\,, \tag{19}$$

and

$$\max\left\{\|x_{TC}(0)\|, \ddot{\gamma}_{d,max}\right\} < \min\left\{\frac{\dot{\gamma}_{i,\max} - \dot{\gamma}_{d,\max}}{\kappa_1 + \kappa_2}, \frac{\ddot{\gamma}_{i,\max}}{3b\kappa_1 + 3b\kappa_2 + 1}\right\}, \tag{20}$$

for given $\dot{\gamma}_{i,\max}, \ddot{\gamma}_{i,\max} > 0$ and for some positive constants κ_1 and κ_2. Then, there exist time coordination control gains a, b and k such that the time-coordination error vector is bounded by

$$||\boldsymbol{x_{TC}}(t)|| \leq \kappa_1 ||\boldsymbol{x_{TC}}(0)|| e^{-\lambda_{TC} t} + \kappa_2 \sup_{t \geq 0}(|\ddot{\gamma}_d(t)|), \tag{21}$$

with rate of convergence satisfying

$$\lambda_{TC} < \frac{n_l}{n}\frac{1}{4b}\frac{\mu}{T\left(1 + \frac{a}{b}nT\right)^2}\,,$$

and such that the feasibility bounds introduced in Equations (4) *and* (5) *are never violated.*

Remark 4 *We note that in a more physical sense, inequality (19) states that the maximum speed of the agents must be greater than the maximum speed of the target. As it will be made clear in the next section, this is due to the fact*

that $\dot{\gamma}_d(t)$ directly depends on the virtual time of the target. Instead, inequality (20) provides an upper bound for the time-coordination error at time $t = 0$.

Proof: The proof of Theorem 1 is provided in Appendix B.

V. Continuous Monitoring Algorithm

Theorem 1 shows that if coordination is achieved, then Equation (7) is satisfied. Furthermore, recall that by virtue of the trajectory generation and virtual target tracking algorithms, the monitoring objectives are met if the following condition is satisfied (see Equation (2)):

$$\gamma_i(t) = \gamma_t(t), \quad \forall i \in \{1, .., n\}. \tag{22}$$

As it was mentioned in Section III, we assume that only a subset of vehicles, the mission leaders, are able to continuously detect the virtual time of the target, $\gamma_t(t)$. Then, the objective of the continuous monitoring algorithm is to design a control law for $\dot{\gamma}_d(t)$ such that satisfaction of Equation (22) is ensured for all agents (both leaders and followers).

To this end, we propose

$$\begin{aligned} \dot{\gamma}_d(t) = 1 + k_p(\gamma_i(t) - \gamma_t(t)) + k_i \int_0^t (\gamma_i(\tau) - \gamma_t(\tau))d\tau, \\ \forall i \in \{1, \ldots, n_l\}. \end{aligned} \tag{23}$$

where k_p and k_i are control gains and $\gamma_t(t)$ is the virtual time of the target.

Then, the following result holds.

Theorem 2 *Let the evolution of $\dot{\gamma}_d(t)$ be governed by the control law proposed in Equation* (23)*. Then, if the assumptions of Theorem 1 hold, we have*

$$\gamma_i(t) \to \gamma_t(t), \qquad \forall i \in \{1, \ldots, n\}. \tag{24}$$

Proof: The proof of Theorem 2 follows directly by substituting Equation (23) into Equation (13) and following similar steps as the proof of Theorem 1.

Remark 5 *We note that when the target is moving with nominal speed and the vehicles are coordinated with the target,*

then $\dot{\gamma}_d(t) = 1$, which in turn implies that the vehicles are progressing at the rate that was originally established at the trajectory generation level. In other words, $\dot{\gamma}_d(t) = 1$ implies that the virtual times progress identically to clock time.

Remark 6 *To achieve coordination, the control law presented in Equation* (23) *needs to ensure that the bounds in* (17) *and* (18) *are satisfied. This, in turn, can be guaranteed by imposing further bounds on the initial conditions of the time-coordination error vector and on the target's speed. This can be seen by the fact that $\ddot{\gamma}_d(t)$, which can be obtained by differentiating Equation* (23)*, depends directly on the speed of the target.*

Remark 7 *We note that with this formulation, the target tracking controller needs only limited knowledge about the target. In fact, the vehicles need to capture only the value of the target's virtual time, which can be computed from the target's position. Thus, information on the target's dynamics, such as speed and acceleration is not required. Moreover, we emphasize that the leaders only need to acquire information about the target. The followers are able to satisfy the target tracking requirement by means of communication with the neighboring vehicles.*

VI. Numerical Results

To prove the efficacy of our method, we present the results obtained from the simulation of a monitoring mission involving 1 target and 3 UAVs. For this scenario, the final mission time is $t_\mathrm{f} = 150\,\mathrm{s}$ and vehicle 3 (shown in yellow) is the leader, while the other agents act as followers (shown in green and blue).

The vehicles are modeled as Dubin's cars and their trajectories are generated offline solving an optimal control problem that satisfies the constraints of Problem 1. The optimal control problem was implemented in MATLAB and run on a Lenovo ThinkPad with Intel Core i7-8550U, 1.80GHz CPU. The computational time with this set-up was approximately 2 s. The nominal trajectory of the target is known, therefore the trajectories are generated such that the UAVs will intercept the target at time intervals $\Delta = 50\,\mathrm{s}$ (see Equation (2)). Furthermore, the trajectories guarantee that a minimum safe distance $d_\mathrm{safe} = 1.5\,\mathrm{m}$ is maintained among the vehicles at all time (see Equation (1)). The nominal vehicle trajectories are shown in Figure 3. We note that these trajectories are planned such that each agent intercepts the target once, where intercepting signifies that the ith vehicle is positioned above the target (see Equation (2)). For the sake of simplicity, in this simulation we focus on a scenario where each agent needs to intercept the target once. However, it can be shown that the coordination results hold for more complex missions. Finally, let the vehicles be equipped with an on-board virtual target tracking algorithm that satisfies Problem 2, with $\dot{\gamma}_{i,max} = 0.3$ and $\ddot{\gamma}_{i,max} = 0.1$, and the time-coordination algorithm presented in Equation (14) where $a = 1.75$, $b = 4.25$, $k = 0.6$, $\dot{\gamma}_{d,max} = 0.25$ and $\ddot{\gamma}_{d,max} = 0.1$.

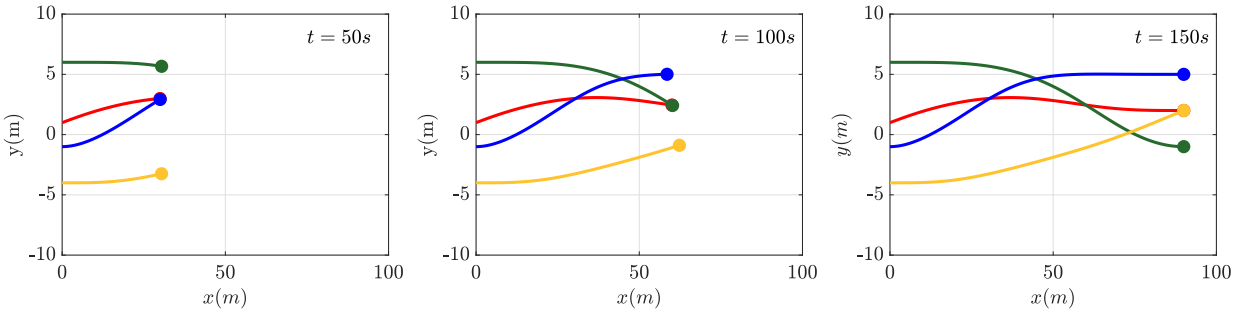

Fig. 3 Target trajectory, shown in red, and agents' trajectories, shown in yellow, blue and green, at three time instances corresponding to target intercept by one of the agents.

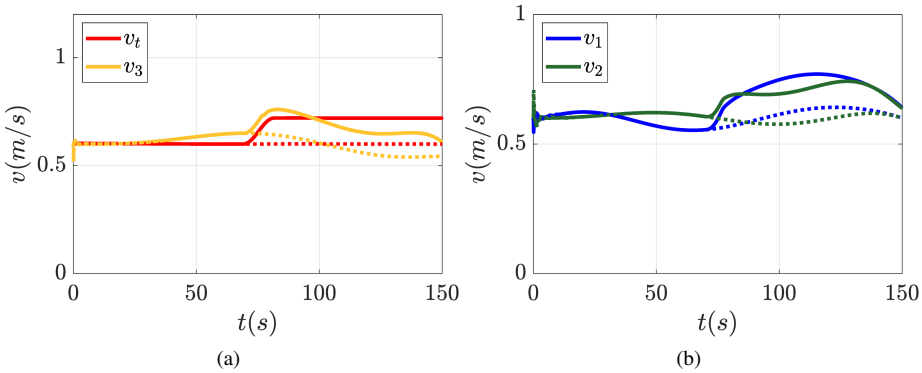

Fig. 4 Speed profile of the target and the leader (left), and speed profile of vehicle 1 and 2 (right). The dotted lines represent the nominal speed of the vehicles; the solid lines show the actual speed of the vehicles.

At the beginning of the mission, the target is following its known nominal trajectory, i.e., $\dot{\gamma}_t(t) = 1$. However, at $t = 70$ s, the target starts speeding up. In turn, by virtue of the PI controller proposed in Equation (23), the desired pace of the mission increases. This implies that the vehicles speed up in order to continue their monitoring task. Figure 4 shows the speed profile of the target and of the vehicles. In Figure 4a, it can be seen that as the target's speed increases, the leader also increases its speed. Figure 4b shows the speed profile of the followers; the followers also adjust their speed by virtue of the time-coordination algorithm.

The latter ensures that both the leader and the followers are able to adjust their pace accordingly (and their speed as a result), i.e., $\dot{\gamma}_1(t) = \dot{\gamma}_2(t) = \dot{\gamma}_3(t) = \dot{\gamma}_d(t)$, as can be seen in Figure 5a. Figure 5b shows the evolution of the virtual time. It can be seen that there is an initial time-coordination error, but by virtue of the time-coordination algorithm, the vehicles are able to coordinate after approximately 5 s as it is shown in Figure 5c. We also note that at $t = 70$ s, when the desired pace of the mission is changed, an error in the virtual time of the leader and the followers can be noticed. However, by virtue of the time-coordination algorithm, the vehicles are able to maintain coordination.

Figure 6 shows the evolution of the mission. The light circles represent the nominal position of the vehicles. It can be seen that without the use of the time-coordination algorithm, if the target changes its speed, the vehicles would not be

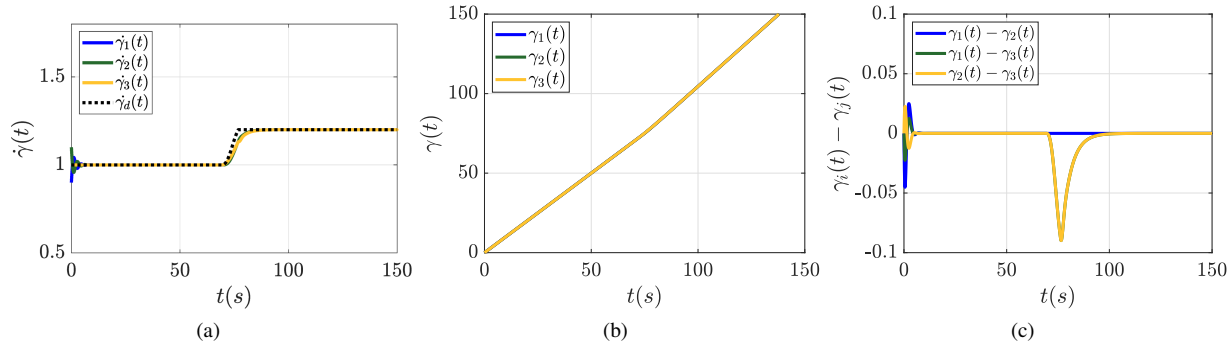

Fig. 5 Evolution of the pace of the mission (left), virtual time (center), and coordination error (right).

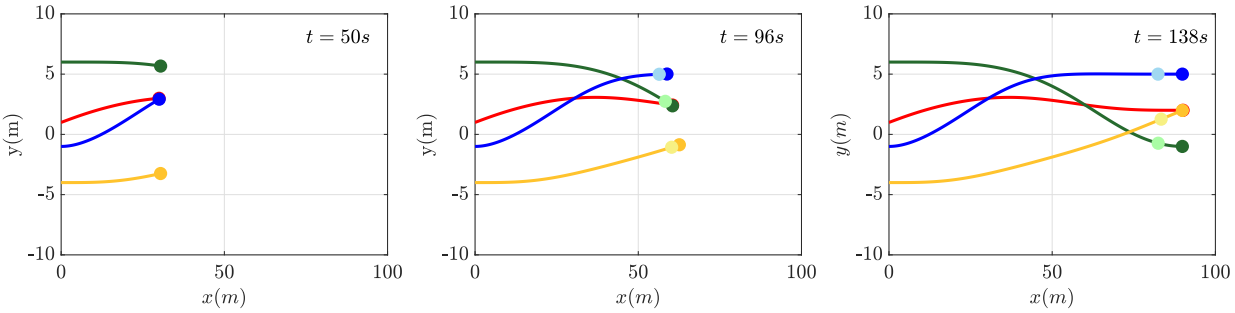

Fig. 6 Target trajectory, shown in red, and agents' trajectories, shown in yellow, blue and green, at three time instances. The nominal positions of the vehicles are shown in a lighter shade of the color.

able to intercept it. Instead, the proposed algorithm ensures that all the agents are able to adjust their speed to complete the mission. Figure 7 shows the magnitude of the virtual target tracking error. Despite an initial error, the vehicles converge to their desired position. Finally, we note that by achieving coordination, the vehicles are able to maintain the minimum safety distance that was planned at the trajectory generation level, as it can be seen in Figure 8.

VII. Conclusions

In this paper, the problem of monitoring continuously a target with unknown speed is presented. The problem is decoupled as an offline optimal trajectory generation problem and an online trajectory adjustment. Optimal trajectories are generated to satisfy mission requirements and dynamic and boundary constraints. Then, the nominal vehicles' trajectories can be modified online through the use of a time-coordination algorithm. This algorithm ensures that coordination and continuous target monitoring are achieved. Finally, performance bounds and simulations results are provided to demonstrate the efficacy of the algorithm. In particular, it is shown how the proposed framework can be deployed to enable a team of fixed-wing UAVs to monitor a ground target moving along a known constrained path with unknown speed. The vehicles are able to adjust their speed online in order to satisfy the temporal requirements of the target monitoring missions, even when information about target's speed is available to a subset of UAVs only. Ongoing

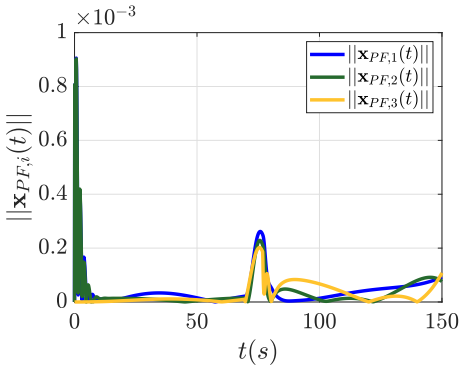

Fig. 7 Evolution of the magnitude of the virtual target tracking error.

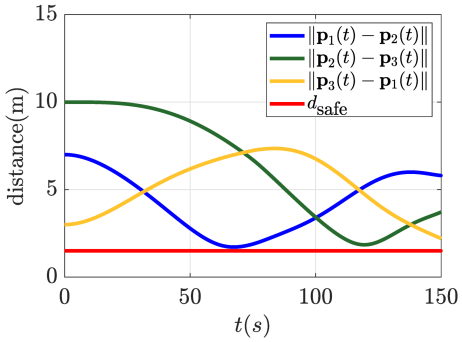

Fig. 8 Distances between the vehicles shown as solid blue, green and yellow lines. The minimum safe distance is shown as a solid red line.

and future work includes effort in nonlinear optimization to enhance the computational efficiency of the trajectory planning algorithm, as well as the implementation of the proposed algorithms on fixed-wing UAVs for real-world testing.

Acknowledgements

This research was supported by the Office of Naval Research, grant N000142112091, with Ms. Christine Buzzell program officer.

References

[1] Michael, N., Stump, E., and Mohta, K., "Persistent Surveillance with a Team of MAVs," *2011 IEEE/RSJ International Conference on Intelligent Robots and Systems*, 2011, pp. 2708–2714. doi:10.1109/IROS.2011.6095174.

[2] Botts, C. H., Spall, J. C., and Newman, A. J., "Multi-Agent Surveillance and Tracking Using Cyclic Stochastic Gradient," *2016 American Control Conference (ACC)*, 2016, pp. 270–275. doi:10.1109/ACC.2016.7524927.

[3] Peters, J. R., Wang, S. J., and Bullo, F., "Coverage Control with Anytime Updates for Persistent Surveillance Missions," *2017 American Control Conference (ACC)*, 2017, pp. 265–270. doi:10.23919/ACC.2017.7962964.

[4] Ehrich Leonard, N., "Cooperative Vehicle Environmental Monitoring," *Springer Handbook of Ocean Engineering*, edited by

M. R. Dhanak and N. I. Xiros, Springer International Publishing, Cham, 2016, pp. 441–458. doi:10.1007/978-3-319-16649-0_19, URL https://doi.org/10.1007/978-3-319-16649-0_19.

[5] Popa, D., Sreenath, K., and Lewis, F., "Robotic Deployment for Environmental Sampling Applications," *2005 International Conference on Control and Automation*, Vol. 1, 2005, pp. 197–202 Vol. 1. doi:10.1109/ICCA.2005.1528116.

[6] Techy, L., Schmale III, D. G., and Woolsey, C. A., "Coordinated Aerobiological Sampling of a Plant Pathogen in the Lower Atmosphere Using Two Autonomous Unmanned Aerial Vehicles," *Journal of Field Robotics*, Vol. 27, No. 3, 2010, pp. 335–343. doi:https://doi.org/10.1002/rob.20335, URL https://onlinelibrary.wiley.com/doi/abs/10.1002/rob.20335.

[7] Smith, S. L., Schwager, M., and Rus, D., "Persistent Robotic Tasks: Monitoring and Sweeping in Changing Environments," *IEEE Transactions on Robotics*, Vol. 28, No. 2, 2012, pp. 410–426. doi:10.1109/TRO.2011.2174493.

[8] Hari, S., Rathinam, S., Darbha, S., Kalyanam, K., Manyam, S., and Casbeer, D., "The Generalized Persistent Monitoring Problem," *2019 American Control Conference (ACC)*, 2019, pp. 2783–2788. doi:10.23919/ACC.2019.8815211.

[9] Hari, S. K. K., Rathinam, S., Darbha, S., Kalyanam, K., Manyam, S. G., and Casbeer, D., "Optimal UAV Route Planning for Persistent Monitoring Missions," *IEEE Transactions on Robotics*, Vol. 37, No. 2, 2021, pp. 550–566. doi:10.1109/TRO.2020.3032171.

[10] Stump, E., and Michael, N., "Multi-Robot Persistent Surveillance Planning as a Vehicle Routing Problem," *2011 IEEE International Conference on Automation Science and Engineering*, 2011, pp. 569–575. doi:10.1109/CASE.2011.6042503.

[11] Peterson, C. K., Casbeer, D. W., Manyam, S. G., and Rasmussen, S., "Persistent Intelligence, Surveillance, and Reconnaissance Using Multiple Autonomous Vehicles With Asynchronous Route Updates," *IEEE Robotics and Automation Letters*, Vol. 5, No. 4, 2020, pp. 5550–5557. doi:10.1109/LRA.2020.3008140.

[12] Cassandras, C. G., Lin, X., and Ding, X., "An Optimal Control Approach to the Multi-Agent Persistent Monitoring Problem," *IEEE Transactions on Automatic Control*, Vol. 58, No. 4, 2013, pp. 947–961. doi:10.1109/TAC.2012.2225539.

[13] Lin, X., and Cassandras, C. G., "An Optimal Control Approach to the Multi-Agent Persistent Monitoring Problem in Two-Dimensional Spaces," *IEEE Transactions on Automatic Control*, Vol. 60, No. 6, 2015, pp. 1659–1664. doi:10.1109/TAC.2014.2359712.

[14] Song, C., Liu, L., Feng, G., and Xu, S., "Optimal Control for Multi-Agent Persistent Monitoring," *Automatica*, Vol. 50, No. 6, 2014, pp. 1663–1668. doi:https://doi.org/10.1016/j.automatica.2014.04.011, URL https://www.sciencedirect.com/science/article/pii/S0005109814001411.

[15] Anderson, R. P., and Milutinović, D., "A Stochastic Approach to Dubins Vehicle Tracking Problems," *IEEE Transactions on Automatic Control*, Vol. 59, No. 10, 2014, pp. 2801–2806. doi:10.1109/TAC.2014.2314224.

[16] Anderson, R., and Milutinovic´, D., "Dubins Vehicle Tracking of a Target With Unpredictable Trajectory," 2011, pp. 675–682. doi:10.1115/DSCC2011-6060, URL https://doi.org/10.1115/DSCC2011-6060.

[17] Baumgartner, K. A. C., Ferrari, S., and Rao, A. V., "Optimal Control of an Underwater Sensor Network for Cooperative Target Tracking," *IEEE Journal of Oceanic Engineering*, Vol. 34, No. 4, 2009, pp. 678–697. doi:10.1109/JOE.2009.2025643.

[18] Haugen, J., and Imsland, L., "Monitoring Moving Objects Using Aerial Mobile Sensors," *IEEE Transactions on Control Systems Technology*, Vol. 24, No. 2, 2016, pp. 475–486. doi:10.1109/TCST.2015.2454432.

[19] Haugen, J., and Imsland, L., "UAV Path Planning for Multitarget Tracking with Experiments*," *IFAC Proceedings Volumes*, Vol. 46, No. 30, 2013, pp. 316–323. doi:https://doi.org/10.3182/20131120-3-FR-4045.00061, URL https://www.sciencedirect.com/science/article/pii/S147466701540312X, 2nd IFAC Workshop on Research, Education and Development of Unmanned Aerial Systems.

[20] Cichella, V., "Cooperative Autonomous Systems: Motion Planning and Coordinated Tracking Control for Multi-Vehicle Missions," Ph.D. thesis, University of Illinois at Urbana-Champaign, 2018.

[21] Mehdi, S. B., Cichella, V., Marinho, T., and Hovakimyan, N., "Collision Avoidance in Multi-Vehicle Cooperative Missions Using Speed Adjustment," *2017 IEEE 56th Annual Conference on Decision and Control (CDC)*, 2017, pp. 2152–2157. doi:10.1109/CDC.2017.8263963.

[22] Tabasso, C., Cichella, V., Mehdi, S. B., Marinho, T., and Hovakimyan, N., "Guaranteed Collision Avoidance in Multivehicle Cooperative Missions Using Speed Adjustment," *Journal of Aerospace Information Systems*, Vol. 17, No. 8, 2020, pp. 436–453. doi:10.2514/1.I010788.

[23] Tabasso, C., Cichella, V., Mehdi, S. B., Marinho, T., and Hovakimyan, N., "Time Coordination and Collision Avoidance Using Leader-Follower Strategies in Multi-Vehicle Missions," *Robotics*, Vol. 10, No. 1, 2021. doi:10.3390/robotics10010034, URL https://www.mdpi.com/2218-6581/10/1/34.

[24] Choe, R., Puig-Navarro, J., Cichella, V., Xargay, E., and Hovakimyan, N., "Cooperative Trajectory Generation Using Pythagorean Hodograph Bézier Curves," *Journal of Guidance, Control, and Dynamics*, Vol. 39, No. 8, 2016, pp. 1744–1763. doi:10.2514/1.G001531.

[25] Cichella, V., Kaminer, I., Walton, C., and Hovakimyan, N., "Optimal Motion Planning for Differentially Flat Systems Using Bernstein Approximation," *IEEE Control Systems Letters*, Vol. 2, No. 1, 2018, pp. 181–186. doi:10.1109/LCSYS.2017.2778313.

[26] Kielas-Jensen, C., and Cichella, V., "BeBOT: Bernstein Polynomial Toolkit for Trajectory Generation," *2019 IEEE/RSJ International Conference on Intelligent Robots and Systems (IROS)*, 2019, pp. 3288–3293. doi:10.1109/IROS40897.2019.8967564.

[27] Cichella, V., Kaminer, I., Dobrokhodov, V., Xargay, E., Choe, R., Hovakimyan, N., Aguiar, A. P., and Pascoal, A. M., "Cooperative Path Following of Multiple Multirotors Over Time-Varying Networks," *IEEE Transactions on Automation Science and Engineering*, Vol. 12, No. 3, 2015, pp. 945–957. doi:10.1109/TASE.2015.2406758.

[28] Xargay, E., Kaminer, I., Pascoal, A., Hovakimyan, N., Dobrokhodov, V., Cichella, V., Aguiar, A., and Ghabcheloo, R., "Time-Critical Cooperative Path Following of Multiple Unmanned Aerial Vehicles Over Time-Varying Networks," *Journal of Guidance, Control, and Dynamics*, Vol. 36, No. 2, 2013, pp. 499–516. doi:10.2514/1.56538.

[29] Cichella, V., Kaminer, I., Walton, C., Hovakimyan, N., and Pascoal, A. M., "Optimal Multivehicle Motion Planning Using Bernstein Approximants," *IEEE Transactions on Automatic Control*, Vol. 66, No. 4, 2021, pp. 1453–1467. doi: 10.1109/TAC.2020.2999329.

[30] Cichella, V., Kaminer, I., Dobrokhodov, V., Xargay, E., Hovakimyan, N., and Pascoal, A., "Geometric 3D Path-Following Control for a Fixed-Wing UAV on SO (3)," *AIAA Guidance, Navigation, and Control Conference*, 2011, p. 6415. doi: 10.2514/6.2011-6415.

[31] Lewis, F. L., Zhang, H., Hengster-Movric, K., and Das, A., *Cooperative Control of Multi-Agent Systems: Optimal and Adaptive Design Approaches*, Springer Science & Business Media, 2013.

[32] Arcak, M., "Passivity as a Design Tool for Group Coordination," *IEEE Transactions on Automatic Control*, Vol. 52, No. 8, 2007, pp. 1380–1390. doi:10.1109/TAC.2007.902733.

[33] Loría, A., and Panteley, E., "Uniform Exponential Stability of Linear Time-Varying Systems: Revisited," *Systems & Control Letters*, Vol. 47, No. 1, 2002, pp. 13–24. doi:https://doi.org/10.1016/S0167-6911(02)00165-2, URL `https://www.sciencedirect.com/science/article/pii/S0167691102001652`.

[34] Khalil, H. K., *Nonlinear Systems*, Prentice Hall, Englewood Cliffs, NJ, 2002.

A. Proof of Time-Coordination Dynamics

Consider the following time-coordination states redefined using the definitions given in (8), (15) and (16):

$$\bar{\boldsymbol{x}}_{\boldsymbol{TC}} = [\boldsymbol{\chi}^\top, \mathbf{z}^\top, \boldsymbol{\zeta}^\top]^\top,$$

where

$$\begin{cases} \mathbf{z} = \dot{\boldsymbol{\gamma}} - \dot{\gamma}_d \mathbf{1}_{\boldsymbol{n}} \\ \boldsymbol{\chi} = b\boldsymbol{\xi} + Q\mathbf{z} \\ \boldsymbol{\zeta} = \boldsymbol{\chi}_{\boldsymbol{I}} - \dot{\gamma}_d \mathbf{1}_{\boldsymbol{n-n_I}} - \frac{k}{a} C^\top Q^\top \boldsymbol{\chi} \end{cases} \tag{25}$$

and

$$\dot{\boldsymbol{\chi}}_{\boldsymbol{I}} = -kC^\top L\boldsymbol{\gamma}. \tag{26}$$

Then, the time-coordination control law can be rewritten as

$$\ddot{\boldsymbol{\gamma}} = -aL\boldsymbol{\gamma} - b\begin{bmatrix} D^\top\dot{\boldsymbol{\gamma}} - \dot{\gamma}_d\mathbf{1}_{\boldsymbol{n_I}} \\ C^\top\dot{\boldsymbol{\gamma}} - \boldsymbol{\chi_I} \end{bmatrix} = -aLQ^\top Q\boldsymbol{\chi} - b\begin{bmatrix} D^\top\dot{\boldsymbol{\gamma}} - \dot{\gamma}_d\mathbf{1}_{\boldsymbol{n_I}} \\ C^\top\dot{\boldsymbol{\gamma}} - \boldsymbol{\chi_I} + \dot{\gamma}_d\mathbf{1}_{\boldsymbol{n-n_I}} - \dot{\gamma}_d\mathbf{1}_{\boldsymbol{n-n_I}} \end{bmatrix}$$
$$= -aLQ^\top Q\boldsymbol{\chi} - b\begin{bmatrix} D^\top\dot{\boldsymbol{\gamma}} - \dot{\gamma}_d\mathbf{1}_{\boldsymbol{n_I}} \\ C^\top\dot{\boldsymbol{\gamma}} - \boldsymbol{\zeta} - \frac{k}{a}C^\top Q^\top\boldsymbol{\chi} - \dot{\gamma}_d\mathbf{1}_{\boldsymbol{n-n_I}} \end{bmatrix} = -\frac{a}{b}LQ^\top\boldsymbol{\chi} + \frac{a}{b}LQ^\top Q\boldsymbol{z} - b\boldsymbol{z} + bC\boldsymbol{\zeta} + \frac{kb}{a}CC^\top Q^\top\boldsymbol{\chi}. \tag{27}$$

Using (25), the time derivative of χ is

$$\dot{\boldsymbol{\chi}} = bQ\dot{\boldsymbol{\gamma}} + Q(\ddot{\boldsymbol{\gamma}} - \ddot{\gamma}_d\mathbf{1}_{\boldsymbol{n}}).$$

Recalling the properties of matrix Q, the equation above can be simplified to

$$\dot{\boldsymbol{\chi}} = bQ\dot{\boldsymbol{\gamma}} + Q\ddot{\boldsymbol{\gamma}}.$$

Using (27), it follows that

$$\dot{\boldsymbol{\chi}} = -\frac{a}{b}\bar{L}\boldsymbol{\chi} + \frac{bk}{a}QCC^\top Q^\top\boldsymbol{\chi} + \frac{a}{b}\bar{L}Q\boldsymbol{z} + bQC\boldsymbol{\zeta}.$$

A similar approach is used to derive the dynamics of z and ζ. Using (25) and straightforward computations, we obtain

$$\dot{\boldsymbol{z}} = -(bI - \frac{a}{b}L)\boldsymbol{z} - \frac{a}{b}LQ^\top\boldsymbol{\chi} + \frac{bk}{a}CC^\top Q^\top\boldsymbol{\chi} + bC\boldsymbol{\zeta} - \ddot{\gamma}_d\mathbf{1}_{\boldsymbol{n}}.$$

Using (25) and (26), we obtain

$$\dot{\boldsymbol{\zeta}} = -kC^\top LQ^\top\left(\frac{1}{b}\boldsymbol{\chi} - \frac{1}{b}Q\boldsymbol{z}\right) - \ddot{\gamma}_d\mathbf{1}_{\boldsymbol{n-n_I}} - \frac{k}{a}C^\top Q^\top\dot{\boldsymbol{\chi}}.$$

The dynamics of ζ can be written as

$$\dot{\boldsymbol{\zeta}} = -\frac{kb}{a}C^\top Q^\top QC\boldsymbol{\zeta} - \frac{bk^2}{a^2}C^\top Q^\top QCC^\top Q^\top\boldsymbol{\chi} - \ddot{\gamma}_d\mathbf{1}_{\boldsymbol{n-n_I}}.$$

Thus, the dynamics presented in (30) are derived.

B. Proof of Theorem 1

First, consider the following system:

$$\dot{\phi}(t) = -\frac{a}{b}\bar{L}\phi(t)\,, \tag{28}$$

where the matrix $\bar{L}$ satisfies the condition of Equation (9). From [33, Lemma 5] it follows that (28) is globally uniformly exponentially stable, and that the following bound holds:

$$||\phi(t)|| \leq k_\lambda ||\phi(0)|| e^{-\gamma_\lambda t}\,,$$

with $k_\lambda = 1$ and $\gamma_\lambda \geq \bar{\gamma}_\lambda = \frac{a}{b}\frac{n\mu}{T(1+\frac{a}{b}nT)^2}$. Using [34, Theorem 4.14], it follows that there exists a continuously differentiable, symmetric, positive definite matrix $P(t)$ that satisfies the inequalities:

$$\begin{aligned} &0 < \bar{c}_1 I \triangleq \frac{\bar{c}_3}{2n} I \leq P(t) \leq \frac{\bar{c}_4}{2\gamma_\lambda} I \triangleq \bar{c}_2 I, \\ &\dot{P} - \frac{a}{b}\bar{L}P - \frac{a}{b}P\bar{L} \leq -\bar{c}_3 I\,. \end{aligned} \tag{29}$$

Recall the time-coordination states derived in Appendix A

$$\begin{aligned} \boldsymbol{\chi} &= b\boldsymbol{\xi} + Q\mathbf{z}, \\ \mathbf{z} &= \dot{\boldsymbol{\gamma}} - \dot{\gamma}_d \mathbf{1}_\mathbf{n}, \\ \boldsymbol{\zeta} &= \boldsymbol{\chi}_{\boldsymbol{I}} - \dot{\gamma}_d \mathbf{1}_{\mathbf{n}-\mathbf{n_l}} - \frac{k}{a} C^\top Q^\top \boldsymbol{\chi}, \end{aligned}$$

with dynamics given by:

$$\begin{cases} \dot{\boldsymbol{\chi}} = -\frac{a}{b}\bar{L}\boldsymbol{\chi} + \frac{bk}{a} QCC^\top Q^\top \boldsymbol{\chi} + \frac{a}{b}\bar{L}Q\mathbf{z} + bQC\boldsymbol{\zeta}, \\ \dot{\boldsymbol{z}} = -(bI - \frac{a}{b}L)z - \frac{a}{b}LQ^\top \boldsymbol{\chi} + \frac{bk}{a} CC^\top Q^\top \boldsymbol{\chi} + bC\boldsymbol{\zeta} - \ddot{\gamma}_d \mathbf{1}_\mathbf{n}, \\ \dot{\boldsymbol{\zeta}} = -\frac{kb}{a} C^\top Q^\top QC\boldsymbol{\zeta} - \frac{bk^2}{a^2} C^\top Q^\top QCC^\top Q^\top \boldsymbol{\chi} - \ddot{\gamma}_d \mathbf{1}_{\mathbf{n}-\mathbf{n_l}}. \end{cases} \tag{30}$$

Consider the following Lyapunov candidate function:

$$V = \boldsymbol{\chi}^\top P \boldsymbol{\chi} + \frac{\beta}{2} z^\intercal z + \frac{a^2}{k^2} \boldsymbol{\zeta}^\intercal \left(C^\top Q^\top CQ\right)^{-1} \boldsymbol{\zeta} = \bar{\boldsymbol{x}}_{\boldsymbol{TC}}{}^\top W \bar{\boldsymbol{x}}_{\boldsymbol{TC}}\,, \tag{31}$$

where $\beta > 0$, P was introduced above, and

$$W = \begin{bmatrix} P & 0 & 0 \\ 0 & \frac{\beta}{2} I & 0 \\ 0 & 0 & \frac{a^2}{k^2} (C^\top Q^\top C Q)^{-1} \end{bmatrix}.$$

Using (30), the time derivative of (31) can be computed to yield:

$$\begin{aligned} \dot{V} = \boldsymbol{\chi}^\top P \Big(-\frac{a}{b} \bar{L} \boldsymbol{\chi} + \frac{bk}{a} Q C C^\top Q^\top \boldsymbol{\chi} + \frac{a}{b} \bar{L} Q \boldsymbol{z} + b Q C \boldsymbol{\zeta} \Big) + \Big(-\frac{a}{b} \boldsymbol{\chi}^\top \bar{L} + \frac{bk}{a} \boldsymbol{\chi}^\top Q C C^\top Q^\top + \frac{a}{b} \boldsymbol{z}^\top \bar{L} Q^\top \\ + b \boldsymbol{\zeta}^\top C^\top Q^\top \Big) P \boldsymbol{\chi} + \boldsymbol{\chi}^\top \dot{P} \boldsymbol{\chi} + \beta \boldsymbol{z}^\top \Big(-\Big(bI - \frac{a}{b} L \Big) \boldsymbol{z} - \frac{a}{b} L Q^\top \boldsymbol{\chi} + \frac{bk}{a} C C^\top Q^\top \boldsymbol{\chi} + b C \boldsymbol{\zeta} - \ddot{\gamma}_d \mathbf{1}_{\boldsymbol{n}} \Big) \\ + \frac{a^2}{k^2} \Big(-\frac{kb}{a} \boldsymbol{\zeta}^\top C^\top Q^\top Q C - \frac{bk^2}{a^2} \boldsymbol{\chi}^\top Q C C^\top Q^\top Q C - \mathbf{1}_{\boldsymbol{n-n_l}}{}^\top \ddot{\gamma}_d \Big) (C^\top Q^\top Q C)^{-1} \boldsymbol{\zeta} \\ + \frac{a^2}{k^2} \boldsymbol{\zeta}^\top (C^\top Q^\top Q C)^{-1} \Big(-\frac{kb}{a} C^\top Q^\top Q C \boldsymbol{\zeta} - \frac{bk^2}{a^2} C^\top Q^\top Q C C^\top Q^\top \boldsymbol{\chi} - \ddot{\gamma}_d \mathbf{1}_{\boldsymbol{n-n_l}} \Big). \end{aligned}$$

Finally, using the fact that $||L|| \leq N$ and $\lambda_{min} (C^\top Q^\top Q C) = \frac{N_L}{N}$, the above inequality implies

$$\begin{aligned} \dot{V} \leq & \boldsymbol{\chi}^\top \left(\dot{P} - \frac{a}{b} P \bar{L} - \frac{a}{b} \bar{L} P + 2 \frac{kb}{a} Q C C^\top Q^\top P \right) \boldsymbol{\chi} - \beta \boldsymbol{z}^\top \left(bI - \frac{a}{b} L \right) \boldsymbol{z} - \frac{a^2}{k^2} \boldsymbol{\zeta}^\top \left(2 \frac{kb}{a} \right) \boldsymbol{\zeta} \\ & + \left(2 \frac{a}{b} n ||P|| + \beta \frac{kb}{a} + \beta \frac{a}{b} n \right) ||\boldsymbol{\chi}|| ||\boldsymbol{z}|| + \Big(2b ||P|| + 2b \Big) ||\boldsymbol{\chi}|| ||\boldsymbol{z}|| + \beta b ||\boldsymbol{z}|| ||\boldsymbol{\zeta}|| \\ & + \left(\beta \sqrt{n} + 2 \frac{a^2}{k^2} \sqrt{n - n_l} \frac{n_l}{n} \right) ||\bar{\boldsymbol{x}}_{\boldsymbol{TC}}|| |\ddot{\gamma}_d|. \end{aligned}$$

Using (29), and after straightforward computations, we obtain:

$$\begin{aligned} \dot{V} \leq & -\left(\bar{c}_3 - 2 \frac{bk}{a} \bar{c}_2 \right) ||\boldsymbol{\chi}||^2 - \beta \left(b - \frac{a}{b} n \right) ||\boldsymbol{z}||^2 - 2 \frac{ba}{k} ||\boldsymbol{\zeta}||^2 + \left(2 \frac{a}{b} n \bar{c}_2 + \beta \frac{kb}{a} + \beta \frac{a}{b} n \right) ||\boldsymbol{\chi}|| ||\boldsymbol{z}|| \\ & + (2b \bar{c}_2 + 2b) ||\boldsymbol{\chi}|| ||\boldsymbol{\zeta}|| + \beta b ||\boldsymbol{z}|| ||\boldsymbol{\zeta}|| + \eta ||\bar{\boldsymbol{x}}_{\boldsymbol{TC}}|| |\ddot{\gamma}_d(t)|, \end{aligned}$$

where $\eta = \beta \sqrt{n} + 2 \frac{a^2}{k^2} \sqrt{n - n_l} \frac{n_l}{n}$. Finally, using $\bar{c}_2 = \frac{\bar{c}_4}{2 \bar{\gamma}_\lambda}$, letting $\bar{c}_4 = \bar{c}_3$, we get

$$\begin{aligned} \dot{V} \leq & -\left(\bar{c}_3 - 2 \frac{bk}{a} \frac{\bar{c}_3}{\gamma_\lambda} \right) ||\boldsymbol{\chi}||^2 - \beta \left(b - \frac{a}{b} n \right) ||\boldsymbol{z}||^2 - 2 \frac{kb}{a} ||\boldsymbol{\zeta}||^2 + \left(\frac{an \bar{c}_3}{b \gamma_\lambda} + \beta \frac{kb}{a} + \beta \frac{a}{b} n \right) ||\boldsymbol{\chi}|| ||\boldsymbol{z}|| \\ & + \left(\frac{b \bar{c}_3}{\gamma_\lambda} + 2b \right) ||\boldsymbol{\chi}|| ||\boldsymbol{\zeta}|| + \beta b ||\boldsymbol{z}|| ||\boldsymbol{\zeta}|| + \eta ||\bar{\boldsymbol{x}}_{\boldsymbol{TC}}|| |\ddot{\gamma}_d|, \end{aligned}$$

which can be written in matrix form as

$$\dot{V} \leq -\bar{\boldsymbol{x}}_{\boldsymbol{TC}}{}^\top M \bar{\boldsymbol{x}}_{\boldsymbol{TC}} + \eta ||\bar{\boldsymbol{x}}_{\boldsymbol{TC}}|| |\ddot{\gamma}_d|,$$

with

$$M = \begin{bmatrix} \bar{c}_3 - \frac{bk}{a}\frac{\bar{c}_3}{\bar{\gamma}_\lambda} & -\left(\frac{a}{b}\frac{n\bar{c}_3}{\bar{\gamma}_\lambda} + \beta\frac{kb}{a} + \beta\frac{a}{b}n\right) & -\left(\frac{b\bar{c}_3}{\bar{\gamma}_\lambda} + 2b\right) \\ -\left(\frac{a}{b}\frac{n\bar{c}_3}{\bar{\gamma}_\lambda} + \beta\frac{kb}{a} + \beta\frac{a}{b}n\right) & \beta\left(b - \frac{a}{b}n\right) & -\beta b \\ -\left(\frac{b\bar{c}_3}{\bar{\gamma}_\lambda} + 2b\right) & -\beta b & 2\frac{ba}{k} \end{bmatrix}.$$

Then, if

$$M - 2\lambda_{TC}W \geq \begin{bmatrix} \bar{c}_3 - \frac{bk}{a}\frac{\bar{c}_3}{\bar{\gamma}_\lambda} - \frac{\bar{c}_3}{\bar{\gamma}_\lambda}\lambda_{TC} & -\left(\frac{a}{b}\frac{n\bar{c}_3}{\bar{\gamma}_\lambda} + \beta\frac{kb}{a} + \beta\frac{a}{b}n\right) & -\left(\frac{b\bar{c}_3}{\bar{\gamma}_\lambda} + 2b\right) \\ -\left(\frac{a}{b}\frac{n\bar{c}_3}{\bar{\gamma}_\lambda} + \beta\frac{kb}{a} + \beta\frac{a}{b}n\right) & \beta\left(b - \frac{a}{b}n\right) - \beta\lambda_{TC} & -\beta b \\ -\left(\frac{b\bar{c}_3}{\bar{\gamma}_\lambda} + 2b\right) & -\beta b & 2\frac{ba}{k} - 2\frac{a^2}{k^2}\frac{n}{n_l}\lambda_{TC} \end{bmatrix} \geq 0, \tag{32}$$

the time derivative of the Lyapunov function is bounded as follows:

$$\dot{V} \leq -2\lambda_{TC}V + \left(\beta\sqrt{n} + 2\frac{a^2}{k^2}\sqrt{n_l}\frac{n_l}{n}\right)||\bar{\boldsymbol{x}}_{\boldsymbol{TC}}||\,|\ddot{\gamma}_d|. \tag{33}$$

It can be demonstrated that by setting $a = \frac{b}{n}$, $k = \frac{1}{4}\frac{\bar{\gamma}_\lambda}{bn}$, $\lambda_{TC} = \delta\bar{\gamma}_\lambda$, $\beta = \frac{2\bar{c}_3}{\bar{\gamma}_\lambda}$, $\bar{c}_3 = \frac{k}{a}$ and $\delta < \frac{n_l}{n}\frac{1}{4b}$, inequality (32) holds for sufficiently large values of b. Therefore, one can conclude that the system (30) is input-to-state stable [34, Lemma 4.6], and the following bound holds:

$$||\bar{\boldsymbol{x}}_{\boldsymbol{TC}}(t)|| \leq \sqrt{\frac{\max\left(\bar{c}_2, \frac{\beta_1}{2}, \frac{a^2}{k^2}\frac{n}{n_l}\right)}{\min\left(\bar{c}_1, \frac{\beta_1}{2}, \frac{a^2}{k^2}\right)}}||\bar{\boldsymbol{x}}_{\boldsymbol{TC}}(0)||e^{-\lambda_{TC}t} + \sqrt{\frac{\max\left(\bar{c}_2, \frac{\beta_1}{2}, \frac{a^2}{k^2}\frac{n}{n_l}\right)}{\min\left(\bar{c}_1, \frac{\beta_1}{2}, \frac{a^2}{k^2}\right)}}\frac{\eta}{2\bar{\gamma}_\lambda \min\left(\bar{c}_1, \frac{\beta_1}{2}, \frac{a^2}{k^2}\right)}\sup_{t\geq 0}|\ddot{\gamma}_d|\,. \tag{34}$$

Finally, from the definition

$$\bar{\boldsymbol{x}}_{\boldsymbol{TC}} \triangleq S\boldsymbol{x}_{\boldsymbol{TC}}\,, \quad S = \begin{bmatrix} bI_{N-1} & Q & 0 \\ 0 & I_N & 0 \\ -\frac{k}{a}C^\top Q^\top & 0 & I_{N-N_L} \end{bmatrix},$$

we can conclude that

$$||\boldsymbol{x}_{\boldsymbol{TC}}(t)|| \leq \kappa_1||\boldsymbol{x}_{\boldsymbol{TC}}(0)||e^{-\lambda_{TC}t} + \kappa_2\sup_{t\geq 0}(|\ddot{\gamma}_d(t)|)\,, \tag{35}$$

with

$$\kappa_1 = ||S^{-1}|| \sqrt{\frac{\max\left(\bar{c}_2, \frac{\beta_1}{2}, \frac{a^2}{k^2}\frac{n}{n_l}\right)}{\min\left(\bar{c}_1, \frac{\beta_1}{2}, \frac{a^2}{k^2}\right)}} ||S||, \tag{36}$$

and

$$\kappa_2 = ||S^{-1}|| \sqrt{\frac{\max\left(\bar{c}_2, \frac{\beta_1}{2}, \frac{a^2}{k^2}\frac{n}{n_l}\right)}{\min\left(\bar{c}_1, \frac{\beta_1}{2}, \frac{a^2}{k^2}\right)}} \frac{\beta\sqrt{n} + 2\frac{a^2}{k^2}\sqrt{n-n_l}\frac{n_l}{n}}{2\bar{\gamma}_\lambda \min\left(\bar{c}_1, \frac{\beta_1}{2}, \frac{a^2}{k^2}\right)}. \tag{37}$$

In conclusion, we need to demonstrate that $\dot{\gamma}_i$ and $\ddot{\gamma}_i$ $\forall i \in \{1 \ldots, N\}$, satisfy the inequalities shown in (4) and (5). From Equation (35) it follows that

$$|\dot{\gamma}_i(t) - 1| \leq |\dot{\gamma}_d(t) - 1| + \kappa_1 ||\boldsymbol{x_{TC}}(0)|| e^{-\lambda_{TC} t} + \kappa_2 \sup_{t \geq 0}(|\ddot{\gamma}_d(t)|).$$

Using (17) and (18), we can write the equation above as

$$|\dot{\gamma}_i(t) - 1| \leq \dot{\gamma}_{d,\max} + (\kappa_1 + \kappa_2) \max\{\|\boldsymbol{x_{TC}}(0)\|, \ddot{\gamma}_{d,\max}\}. \tag{38}$$

Finally, the assumptions given by Equations (19) and (20) allow us to conclude that inequality (4) holds. Now we consider bounds on $\ddot{\gamma}_i(t)$. From Equation (27) we get

$$|\ddot{\gamma}_i| \leq b||z|| + b||\zeta|| + +an \max_{j \in \mathcal{N}_i} |\gamma_i(t) - \gamma_j(t)|.$$

Recalling that $b = aN$, it follows that

$$|\ddot{\gamma}_i(t)| \leq 3b\|\boldsymbol{x_{TC}}(t)\|.$$

Using (35), it can be seen that $\ddot{\gamma}_i(t)$ remains bounded as follows:

$$|\ddot{\gamma}_i(t)| \leq (3b\kappa_1 + 3b\kappa_2 + 1) \max\left\{\|\boldsymbol{x_{TC}}(0)\|, \ddot{\gamma}_{d,\max}\right\}. \tag{39}$$

The above inequality, together with Equations (19) and (20), imply that inequality (5) holds, which completes the proof of Theorem 1.